

**On a possibility to extract a signal
 from heavy gluino cascade decays via isolated muon detection
 at the LHC energies**

V. I. Klyukhin, A. A. Neushkin, A. A. Sokolov

SINP, Lomonosov Moscow State University, Moscow, Russia

E-mail: Vyacheslav.Klyukhin@cern.ch

Institute for High Energy Physics, Protvino, Moscow reg., Russia

E-mail: sokolov_a@ihep.ru

Abstract

800 GeV gluino pair production is simulated using ISASUSY 1.1 MC-program. The cascade decay of the gluino into two lightest neutralinos, $\tilde{g} \rightarrow \tilde{\chi}_2^0 X$, $\tilde{\chi}_2^0 \rightarrow \mu^+ \mu^- \tilde{\chi}_1^0$, is studied for a convenient set of SUSY parameters: $\mu = -200$ GeV, $\tan \beta = 2$, average squark masses of 1600 GeV, charged Higgs mass of 500 GeV, and top quark mass of 140 GeV. With such parameters the mass difference between $\tilde{\chi}_2^0$ and $\tilde{\chi}_1^0$ is less than the mass of Z . As a background, $t\bar{t}$, $Z + jets$, WW , WZ and ZZ events were generated using ISAJET 6.50 MC-program. The granularities and energy resolutions of the calorimeters in the pseudorapidity range of $|\eta| < 5$ are taken into account. If missing transverse momentum is greater than 200 GeV, the number of jets in the calorimeters is 4 or more, the invariant mass of two isolated muons is less than 80 GeV, the background in the muon transverse momentum distribution is negligible.

Introduction

The purpose of this paper is to investigate whether it is possible to extract a signal from the heavy gluino decay via the cascade chain

$$\tilde{g} \rightarrow \tilde{\chi}_2^0 q \bar{q}, \quad \tilde{g} \rightarrow \tilde{\chi}_2^0 g, \quad (1)$$

$$\tilde{\chi}_2^0 \rightarrow Z^* \tilde{\chi}_1^0 \rightarrow l^+ l^- \tilde{\chi}_1^0 \quad (l = e, \mu) \quad (2)$$

for the standard SUSY parameters used for the gluino production studies in the ATLAS Letter of Intent [1]. An interest in these cascade decays is caused by the previous investigations [2] in which a possibility to estimate the mass of $\tilde{\chi}_2^0$ by measuring the transverse momentum distribution of the muons coming from the decay (2) was demonstrated at

the UNK energies. Using MC-program ISAJET [3] for their simulations, the authors of [2] showed that the position of the maximum in the muon p_T -distribution reflects the relationship between the masses of $\tilde{\chi}_2^0$ and $\tilde{\chi}_1^0$ as follow:

$$p_{T\mu}^{max} = \frac{m_{\tilde{\chi}_2^0}^2 - m_{\tilde{\chi}_1^0}^2}{4m_{\tilde{\chi}_2^0}} \quad (3)$$

In the present paper we repeat those studies at the LHC energy using the new MC-program ISASUSY 1.1 [4] to generate the signal from gluino pair production, and ISAJET 6.50 [3] to simulate all backgrounds to this signal. We pay special attention to such parameters of the central and forward calorimeters as granularity and energy resolution.

ISASUSY 1.1 was modified to generate not only the signal from the decays of $\tilde{g} \rightarrow X$, but also from the forced decays (1)-(2) directly. As backgrounds to these processes we consider the production of $t\bar{t}$, $Z + jets$ and WW , WZ , ZZ continuum at high transverse momenta with subsequent decays into leptons (i.e. $t \rightarrow Wb$, $W \rightarrow l\nu$, $b \rightarrow X$, $Z \rightarrow ll$, where $l = \mu, \tau$ and $\tau \rightarrow \mu\nu\nu$).

The choice of SUSY parameters

The present status of the minimal SUSY extension of the Standard Model (MSSM) [5] gives us a set of model parameters as follow:

- the gluino mass, $m_{\tilde{g}}$, and an average squark mass, $m_{\tilde{q}}$;
- the Higgs-higgsino mass term, μ ;
- the ratio of the vacuum expectation values of two Higgs doublets required by the MSSM, $\tan\beta$;
- the mass of the charged Higgs particle, m_{H^+} .

In this paper we use the following set of SUSY parameters at the c.m. energy of 16 TeV: $m_{\tilde{g}} = 800$ GeV, $m_{\tilde{q}} = 2m_{\tilde{g}}$, $\mu = -200$ GeV, $\tan\beta = 2$, and $m_{H^+} = 500$ GeV. In addition to this set of parameters we input the value of the top quark mass, the last unknown parameter of the Standard Model, $m_t = 140$ GeV. For those parameters the calculations of the sparticle masses and branching ratios performed in the framework of ISASUSY 1.1 show that the mass difference of two lightest neutralinos, $m_{\tilde{\chi}_2^0} - m_{\tilde{\chi}_1^0}$, is less than the mass of the real Z . Moreover, this difference remains less than the real Z mass in the wide range of $m_{\tilde{g}}$ and μ , as shown in Figs. 1-9. This leads to a natural wish to try to extract a signal from the cascade decays (1)-(2) of heavy gluinos at the chosen set of SUSY parameters.

As Figs. 10-15 display, the ISASUSY 1.1 gives branching ratios for the decays (1) and (2) quite acceptable to detect the leptons coming from the decays (2). Further we will consider the decay mode of $\tilde{\chi}_2^0 \rightarrow \mu^+\mu^-\tilde{\chi}_1^0$ as the basic one, but all our calculations are valid for both leptons mentioned above.

The calorimeter simulation

We assume the R-parity conservation, and that $\tilde{\chi}_1^0$ is the lightest supersymmetric particle (LSP) which escapes the apparatus. This causes high missing transverse momentum in the events with heavy gluino pairs. It is of interest to study the influence of the calorimeter performance to this kinematic variable.

To simulate the calorimeter, particle energies were deposited in the grids with different energy smearings and different granularities in (η, ϕ) -space, depending on the η coverage, where η and ϕ denote the pseudorapidity and azimuthal angle. In the central region, $|\eta| < 3$, we used a cell size of $\Delta\eta \times \Delta\phi = 0.1 \times 0.1$ for both electromagnetic and hadronic central calorimeters. Their energy resolutions were taken as $(\Delta E/E)_{em} = 10\%/\sqrt{E} \oplus 1\%$ and $(\Delta E/E)_{had} = 50\%/\sqrt{E} \oplus 3\%$, respectively. All neutrinos and LSP's, and also muons and electrons originated from W, Z and sparticles (including intermediate τ decays) were not detected in the central calorimeters. The transverse momenta of such electrons and muons were then added to the transverse energies of the calorimeter cells, E_T , to determine the missing transverse momentum from the calorimeter measurements. The muon and electron momentum resolutions were not taken into account.

In the backward-forward region, $3 < |\eta| < 5$, we used the granularity of 0.2×0.2 and energy smearings of $(\Delta E/E)_{em} = 60\%/\sqrt{E} \oplus 1000\%/E \oplus 30\%$ and $(\Delta E/E)_{had} = 150\%/\sqrt{E} \oplus 1000\%/E \oplus 7\%$. In this case all neutrinos and LSP's, and also muons from W, Z and sparticle decays were removed from the forward calorimeter, but not electrons, whose energies were smeared inside the cells in accordance with the chosen electromagnetic resolution. The transverse momenta of muons were not added to the transverse energies of calorimeter cells, taking into account the muon system coverage ($|\eta| < 3$).

We specially used the worst case of hadronic and especially electromagnetic resolutions to simulate the backward-forward region in order to look at the influence on the missing transverse momentum resolution from these effects. Figs. 16-19 demonstrate the p_T^{miss} for the signal and background events with two opposite sign isolated muons for two different η coverages (the criterion of the muon isolation is described below). Here and below we will indicate the distributions in the Figures as follow:

- by *thin solid line* – the events from $\tilde{g} \rightarrow X$ decays;
- by *thick solid line* – the events from the forced (1)-(2) decays;
- by *dashed line* – the events from $t\bar{t}$ background;
- by *dot-dashed line* – the events from Drell-Yan $Z + jets$ production;
- by *dotted line* – the events from WW, WZ and ZZ continuum.

In Fig. 16 the value of missing transverse momentum is determined by sum of all stable charge particle and γ -ray transverse momenta over all η range. In Fig. 17 the same is done for $|\eta| < 5$. The p_T^{miss} distribution in Fig. 18 is obtained from the sum of cell E_T in the central calorimeters only, and from the sum of the transverse momenta of charged leptons not deposited in these calorimeters. Finally, Fig. 19 shows the p_T^{miss} distribution obtained from the sum of cell E_T in the range of $|\eta| < 5$ and the sum of p_T of charged leptons in the central region. One can see that Figs. 19 and 17 are very similar, so the

calorimeter performance does not influence the missing p_T measurements much neither for the signal nor for the backgrounds except for $Z + jets$ production.

The second important signature of the signal events is a presence of several quark jets with high transverse energy. A standard jet algorithm found the cell with the highest E_T (larger than 3 GeV), used this cell to define the axis of jet and collected all the energy in a cone with a size of $\Delta R = \sqrt{(\Delta\eta)^2 + (\Delta\phi)^2} = 0.7$ to estimate the jet energy. Only cells with $E_T > 1$ GeV were considered in this procedure. If the transverse energy of the jet was larger than 100 GeV, the jet was retained as a calorimeter jet. Fig. 20 shows the distribution of the number of calorimeter jets with $E_T > 100$ GeV in the signal and background events with two opposite sign isolated muons.

The cuts applied to the signal and background events

Now we are in a position to describe the cuts applied to the generated events to reduce the backgrounds with respect to the signal. We generated two kinds of the signal events: a sample of events with two gluinos decaying via all possible channels, and a sample of events in which one gluino decays via the cascade chain (1)-(2). The cross-sections and the numbers of such events corresponded to one LHC year are presented in the first two columns of Table 1. The other columns of Table 1 relate to the generated background events caused by standard physics processes. To efficiently generate sufficient background process statistics, we used the partons cuts, shown in brackets in Table 1.

Table 1

Accumulated cut efficiencies for the signal and backgrounds

	$\tilde{g} \rightarrow X$	$\tilde{g} \rightarrow \tilde{\chi}_2^0 X$ $\rightarrow \mu\mu\tilde{\chi}_1^0 X$	$t\bar{t}$ $(p_T^{top,Z} > 200 \text{ GeV})$	$Z + jets$	WW $(p_T^{W,Z} > 100 \text{ GeV})$	WZ	$ZZ\uparrow$
Production cross-section (pb)	2.41	0.0121	302	76.9	5.93	2.51	1.13
Events per $10^5 pb^{-1}$ (with at least 2 muons in backgrounds) \ddagger	241000	977	417330	214390	7347	866	1240
Events passing successive cuts:							
– 2 isolated muons with $p_T > 7 \text{ GeV}$	$\frac{2272}{0.943\%}$	$\frac{333}{34.1\%}$	$\frac{150838}{36.1\%}$	$\frac{158358}{73.9\%}$	$\frac{4960}{67.5\%}$	$\frac{195}{22.5\%}$	$\frac{923}{74.5\%}$
– $p_T^{miss} > 200 \text{ GeV}$	$\frac{1132}{0.47\%}$	$\frac{166}{17.0\%}$	$\frac{3898}{0.934\%}$	$\frac{859}{0.401\%}$	$\frac{45}{0.612\%}$	$\frac{13}{1.5\%}$	$\frac{127}{10.2\%}$
– $n_j > 3$	$\frac{408}{0.169\%}$	$\frac{79}{8.09\%}$	$\frac{34}{0.00815\%}$	$\frac{9}{0.0042\%}$	—	—	—
– $m_{\mu\mu} < 80 \text{ GeV}$	$\frac{208}{0.0863\%}$	$\frac{76}{7.78\%}$	$\frac{14}{0.00335\%}$	$\frac{9}{0.0042\%}$	—	—	—

\uparrow Only $(Z \rightarrow \mu\mu)(Z \rightarrow \nu\nu)$ pair decays are forced for this channel

\ddagger An efficiency of 90% is assumed for muon identification

One should note that the number of events in the second sample consists of only 0.4% of the full number of pair gluino events. Since we concentrate on the decays (1)-(2),

we expect a large background to these channels from other gluino decays giving muons in the final state (e.g. the decays of $\tilde{g} \rightarrow tX$ produce the muons with p_T -distribution close to that one from the decays (1)-(2)). To reduce such background we demand the presence in the range of $|\eta| < 3$ of exactly two opposite sign isolated muons with $p_T > 7$ GeV. The cut on p_T corresponds to the ATLAS inner tracker performance. The isolation criterion for the muon is that no cell with $E_T > 2$ GeV and no track with $p_T > 7$ GeV is present in a cone of $\Delta R = 0.3$ around the muon track. The second part of this criterion forces the first one for the central cell of the cone, whose E_T is ignored.

As shown in Table 1 and in Figs. 16-19, this cut efficiently reduces the number of events in the first signal sample, but does not effect the backgrounds from the standard physics processes so much. For both signal samples Fig. 21 shows the invariant mass distributions for the muons originating from the same $\tilde{\chi}_2^0$ in an event. The similarity of these distributions demonstrate the similar numbers of decays (2) in both samples after the application of the muon isolation cut.

The next three cuts reduce background from the standard physics processes to a negligible level. They are:

- the cut on the missing transverse momentum – $p_T^{miss} > 200$ GeV;
- the cut on the number of jets in the calorimeters – $n_j > 3$;
- the cut on the invariant mass of two opposite sign isolated muons – $m_{\mu\mu} < 80$ GeV.

The effect of these cuts is reflected in Table 1 and in Figs. 22-24. From Figs. 24 and Table 1 one can see that, first, the signal from the gluino production is clearly seen, and, second, when even all cuts are applied, the number of events from the decays of $\tilde{g} \rightarrow X$ is almost three times larger than the number of events from decays (1)-(2). This is caused mainly by the presence of muons originating from W produced by top quark and chargino decays.

The composition of the events in the muon transverse momentum distribution shown in Fig. 24 for $\tilde{g} \rightarrow X$ decays are as follow:

- 32.7% – $\tilde{g} \rightarrow \tilde{\chi}_2^0 X, \tilde{\chi}_2^0 \rightarrow \tilde{\chi}_1^0 \mu\mu$;
- 28.8% – $\tilde{g} \rightarrow \tilde{\chi}_2^\mp t/\bar{t}, \tilde{\chi}_2^\mp \rightarrow \tilde{\chi}_1^0 W, t \rightarrow Wb, W \rightarrow \mu\nu$;
- 7.7% – $\tilde{g} \rightarrow \tilde{\chi}_1^\mp t/\bar{t}, \tilde{\chi}_1^\mp \rightarrow \tilde{\chi}_1^0 W, t \rightarrow Wb, W \rightarrow \mu\nu$;
- 5.8% – $\tilde{g} \rightarrow \tilde{\chi}_4^0 X, \tilde{\chi}_4^0 \rightarrow \tilde{\chi}_1^0 h, h \rightarrow \mu\mu$;
- 15.4% – cascade decays in which muons came not from one but from both gluinos;
- 9.6% – $\tilde{g} \rightarrow t\bar{t}\tilde{\chi}^0, t \rightarrow Wb, W \rightarrow \mu\nu$.

The shapes of the muon p_T -distributions in all these channels are very similar. So we can speak about the detection of the muons from different types of gluino cascade decays. The decays in which the muons originated not from cascade gluino decays give a contribution in p_T -distribution at the level of 9.6% only.

Comparisons with the previous studies

$E_T^{miss} +$ jets signature was studied in [6] where it was shown that to observe a signal from the heavy gluino it is enough to have at least 3 jets with $E_T > 200$ GeV, a fourth

jet with $E_T > 100$ GeV, a circularity $C > 0.2$, and $E_T^{miss} > 300$ GeV. In [7] the isolated muon transverse momentum distributions were investigated for same sign and for opposite sign dileptons for events with $E_T^{miss} > 100$ GeV. To compare our results with both these previous investigations we used our sample of $\tilde{g} \rightarrow X$ decays (48800 events generated), and a newly generated sample of 50000 $t\bar{t}$ production events with all subsequent decays.

Figs. 25 and 26 show E_T^{miss} -distributions obtained from central and forward calorimeter simulations for gluino signal and for $t\bar{t}$ background from those two samples, respectively.

Four histograms are plotted for different sets of cuts in each Figure. Here and below P-cuts denote the cuts from [6] mentioned above. Then, for KK-cuts according to [7] we demand the presence in the event of $E_T^{miss} > 100$ GeV and at least one either same sign (SS) or opposite sign (OS) dimuon. In these cases the isolated muons in dimuons have transverse momentum greater than 30 GeV and $|\eta| < 3$. As an isolation criterion we used the one described above. Finally, KNS-cuts mean our cuts described in previous sections of this note.

The numbers of the events shown in the histograms in Figs. 25-26 and also in Table 2 correspond to the integrated luminosity of $10^5 pb^{-1}$.

Table 2

Event rates expected per $10^5 pb^{-1}$ for different cuts

	P-cuts	KK-cuts, SS	KK-cuts, OS	KNS-cuts, OS
$\tilde{g} \rightarrow X$	14800	930	2540	272
$t\bar{t} \rightarrow X$	1810	2420	61000	< 600

In a similar way the muon transverse momentum distributions are plotted in Figs. 27 and 28. The numbers of muons corresponding to the integrated luminosity of $10^5 pb^{-1}$ are presented in histograms in these Figures and in Table 3. An efficiency of 90% is assumed for muon identification.

Table 3

Isolated mion rates expected per $10^5 pb^{-1}$ for different cuts †

	P-cuts	KK-cuts, SS	KK-cuts, OS	KNS-cuts, OS
$\tilde{g} \rightarrow X$	1900	1030	3020	440
$t\bar{t} \rightarrow X$	< 600	1210	85200	< 600

† An efficiency of 90% is assumed for muon identification

From Tables 2 and 3 one can conclude that the additional demand to detect exactly two opposite sign isolated leptons in the events gives a good opportunity to observe a signal from the heavy gluino production in E_T^{miss} - and in isolated muon p_T -distributions. The numbers we obtained applying P-cuts or KK-cuts to our samples are in consistence with the previous studies [6, 7].

Conclusions and further steps

We conclude, therefore, that the combination of $E_T^{miss} +$ jets cuts with the detection of exactly one opposite sign dilepton is very promising signature to reduce the backgrounds

to the heavy gluino pair production. The cuts applied to the decays of $\tilde{g} \rightarrow X$ and to the background events are enough to extract a SUSY signal over Standard Model background. They are however not enough to extract a signal from the cascade decays (1)-(2) from other heavy gluino decays. A possible improvement could be found by better cut optimizations and more careful investigation of the muon isolation in both signal samples. Another way could be to tag b-quark from the decay of $t \rightarrow Wb$. The results obtained in present paper can also change when the pile-up effect and muon momentum resolution will be included in consideration.

Acknowledgements. The authors are thankful to P. Jenni, D. Froidevaux and S. Hellman for the support of this work and prolific discussions.

References

- [1] ATLAS Letter of Intent, CERN/LHCC/92-4, LHCC/I 2, Geneva, 1992.
- [2] A. A. Neushkin, A. A. Sokolov, G. G. Volkov, *Search for SUSY particles at the UNK energies*. IHEP Preprint 92-70, Protvino, 1992.
- [3] ISAJET 6.50 written by F. E. Paige and S. D. Protopopescu.
- [4] ISASUSY 1.1 written by H. Baer, F. E. Paige, S. D. Protopopescu, and X. Tata.
- [5] H. P. Nilles, Phys. Rep. 110 (1984) 1;
G. Ridolfi, G. C. Ross, F. Zwirner, in Proceedings of Large Hadron Collider Workshop, Aachen 4-9 October 1990, edited by G. Jarlskog and D. Rein, CERN 90-10, ECFA 90-133, Vol. II, p. 608.
- [6] G. Polesello, *Search for gluino pair production in the $E_T^{miss} + jets$ channel*. ATLAS Internal Note PHYS-No-16, 29 January 1993.
- [7] K. Kawagoe and S. Komamiya, *Search for gluino pair production through their cascade decay into same sign dileptons*. ATLAS Internal Note PHYS-No-14, 13 January 1993.

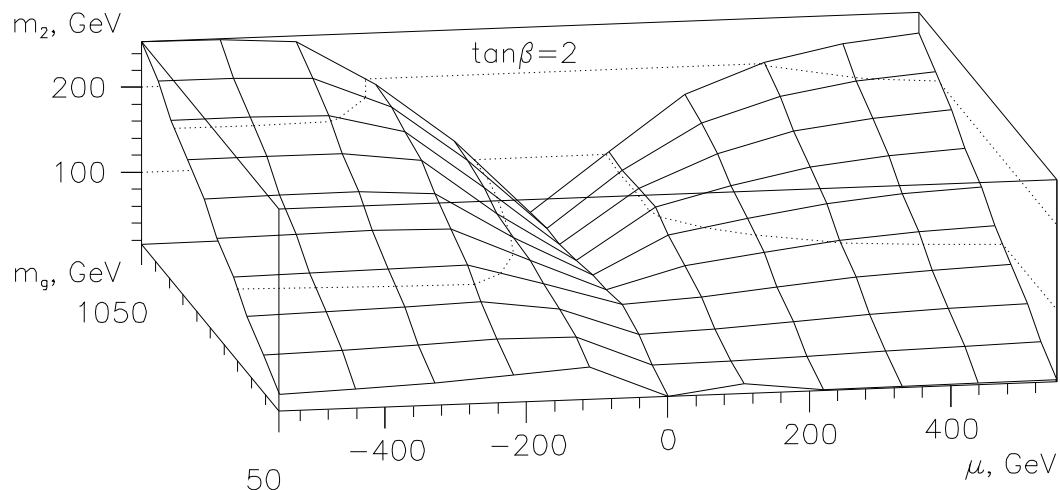


Fig. 1. χ_2^0 mass vs μ and gluino mass.

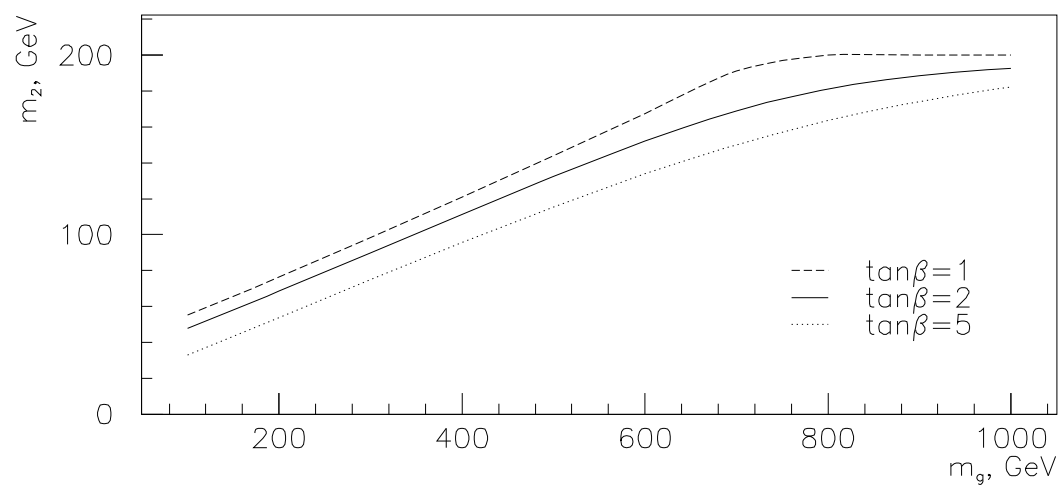


Fig. 2. χ_2^0 mass vs gluino mass for $\mu = -200$ GeV.

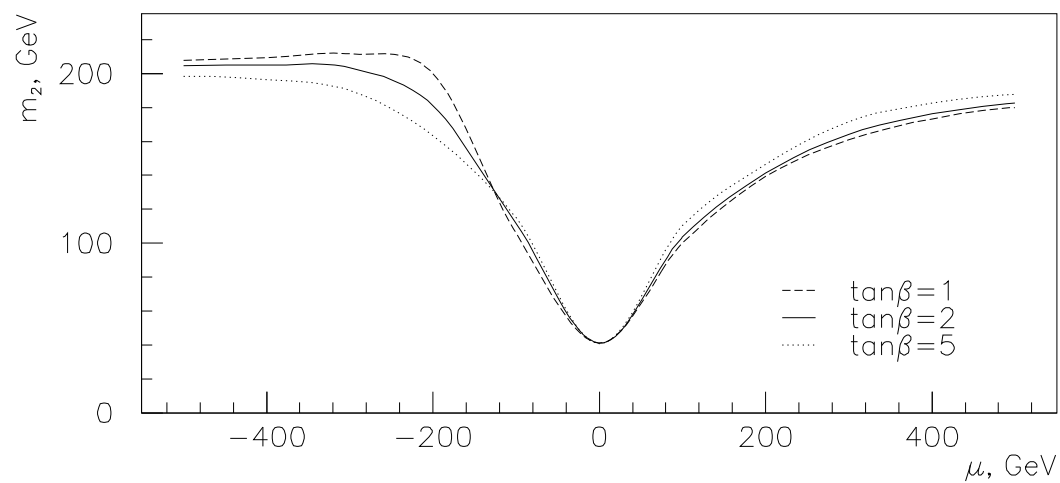


Fig. 3. χ_2^0 mass vs μ for $m_g = 800$ GeV.

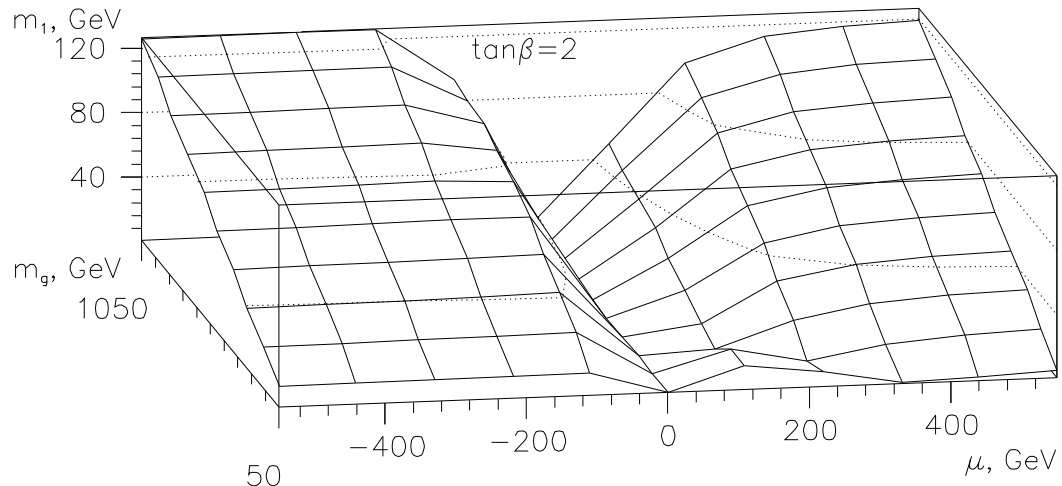


Fig. 4. χ_1^0 mass vs μ and gluino mass.

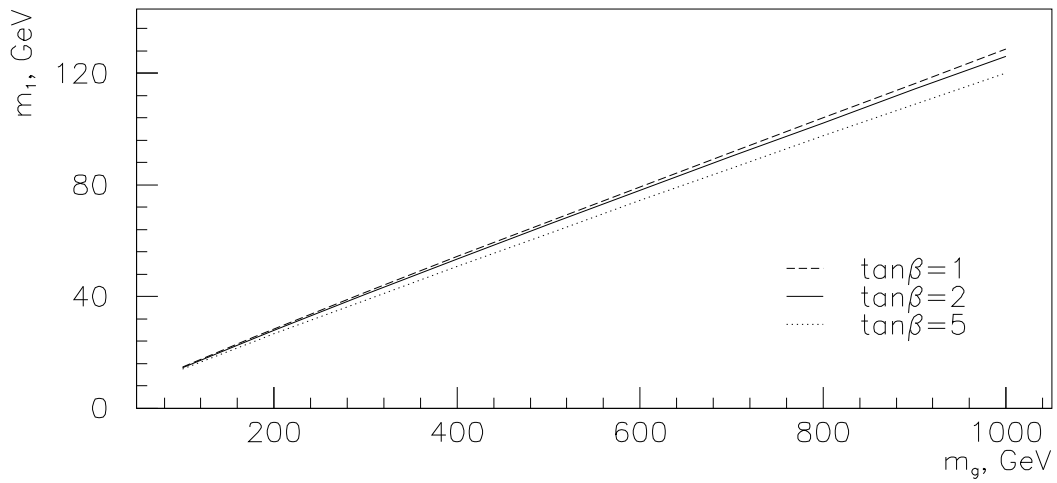


Fig. 5. χ_1^0 mass vs gluino mass for $\mu = -200$ GeV.

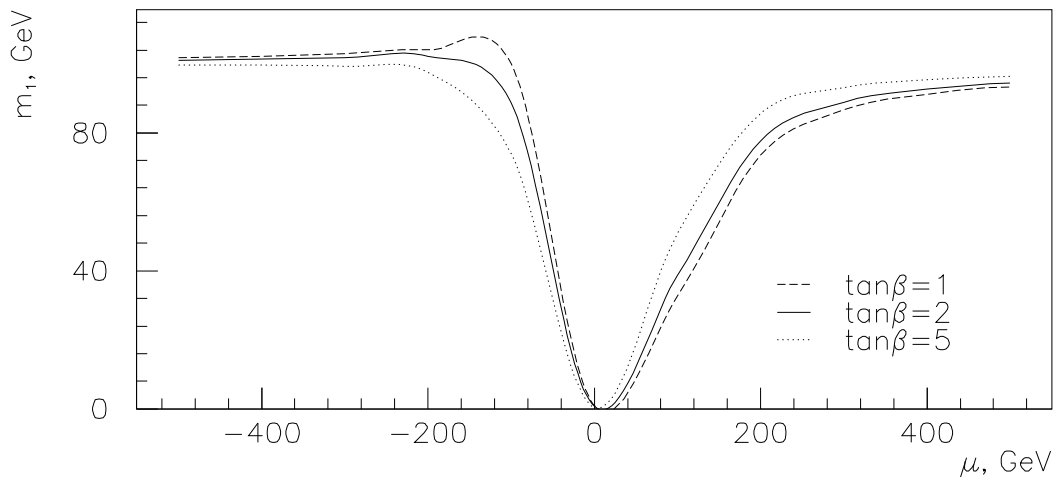


Fig. 6. χ_1^0 mass vs μ for $m_g = 800$ GeV.

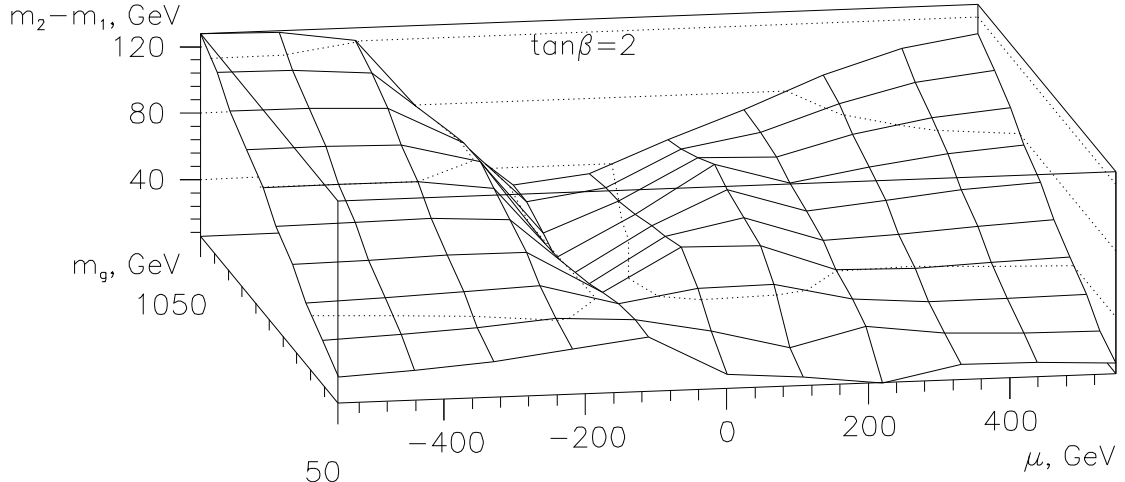


Fig. 7. $\chi_2^0 - \chi_1^0$ mass difference vs μ and gluino mass.

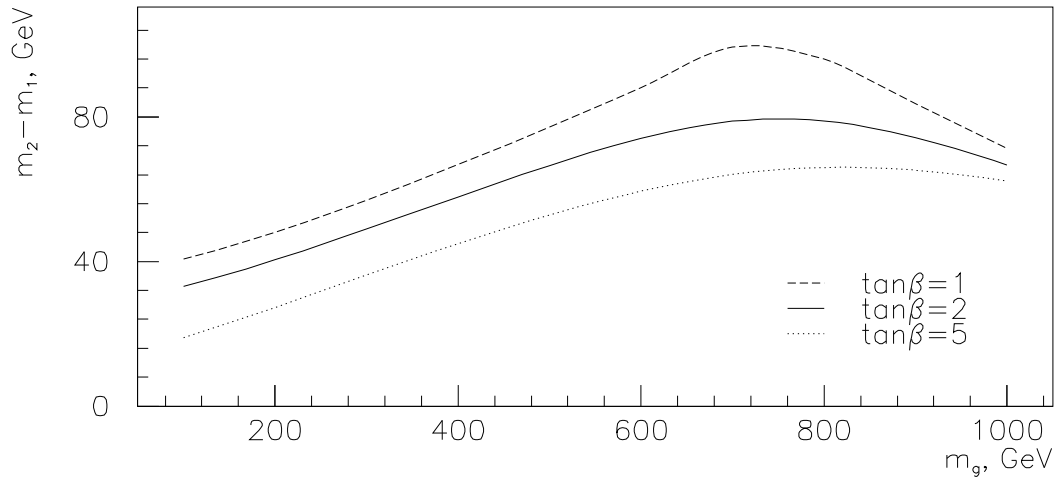


Fig. 8. $\chi_2^0 - \chi_1^0$ mass difference vs m_g for $\mu = -200$ GeV.

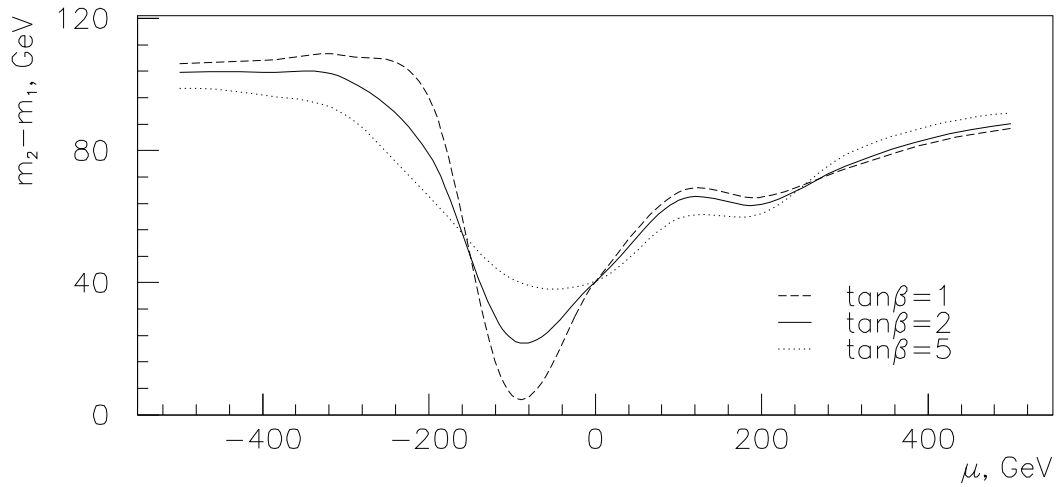


Fig. 9. $\chi_2^0 - \chi_1^0$ mass difference vs μ for $m_g = 800$ GeV.

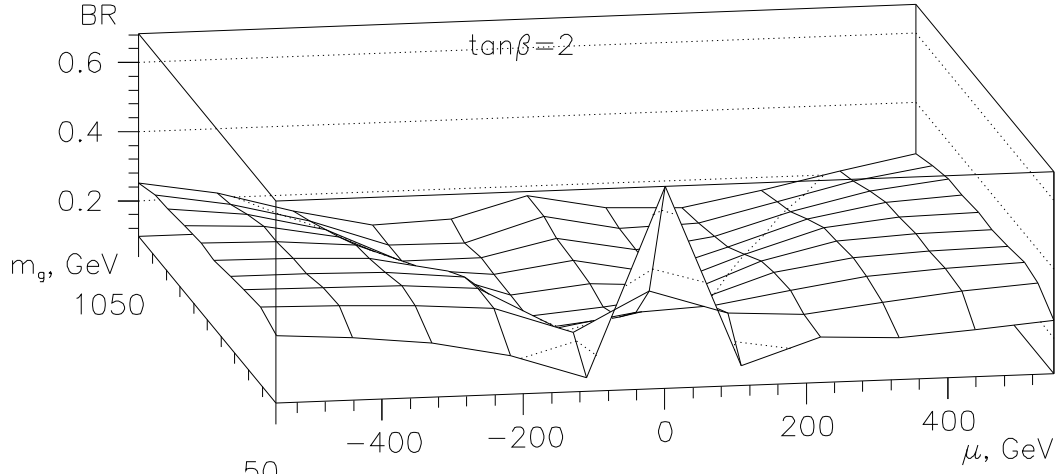


Fig. 10. BR(gluino $\rightarrow \chi_2^0 q \bar{q}$) vs μ and gluino mass.

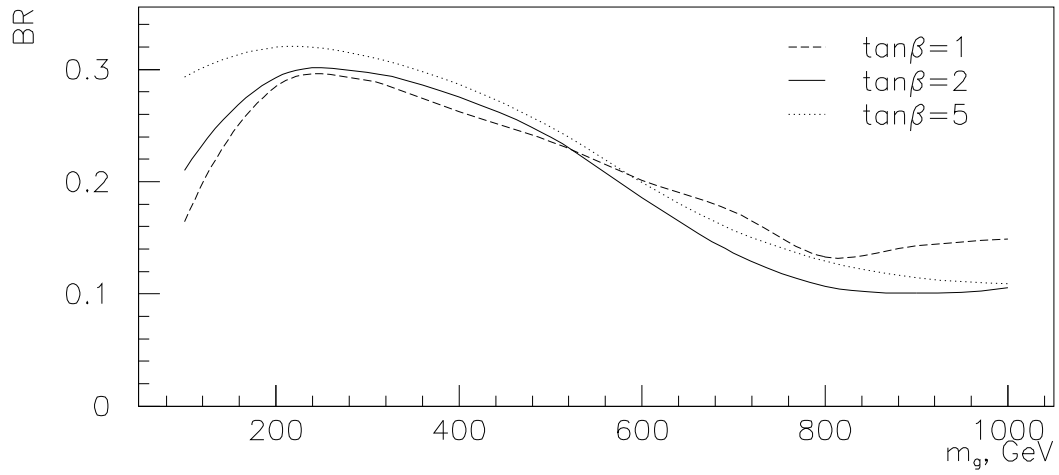


Fig. 11. BR(gluino $\rightarrow \chi_2^0 q \bar{q}$) vs gluino mass for $\mu = -200$ GeV.

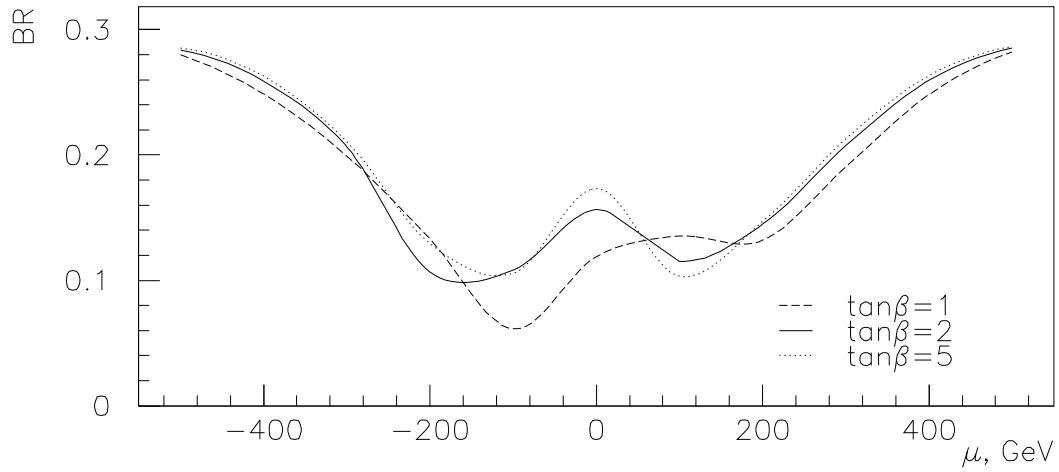


Fig. 12. BR(gluino $\rightarrow \chi_2^0 q \bar{q}$) vs μ for $m_g = 800$ GeV.

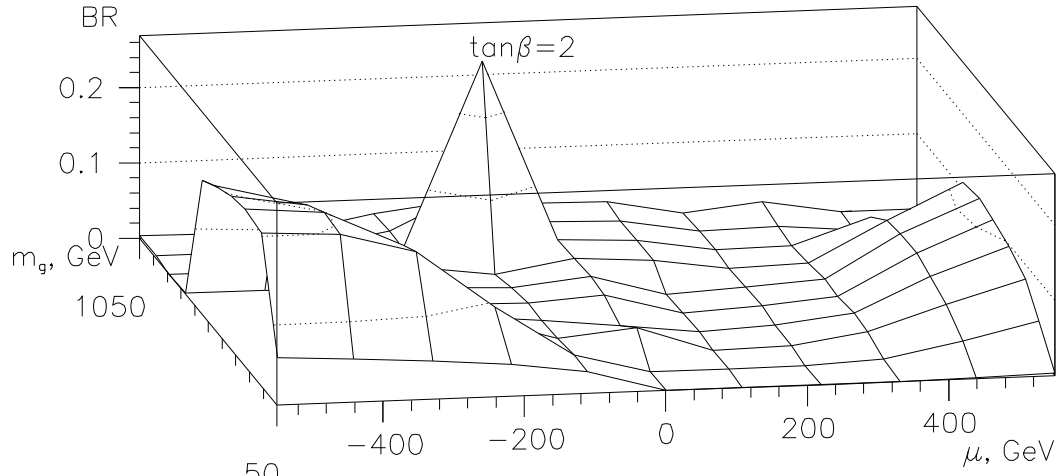


Fig. 13. $BR(\chi_2^0 \rightarrow \chi_1^0 \mu^+ \mu^-)$ vs μ and gluino mass.

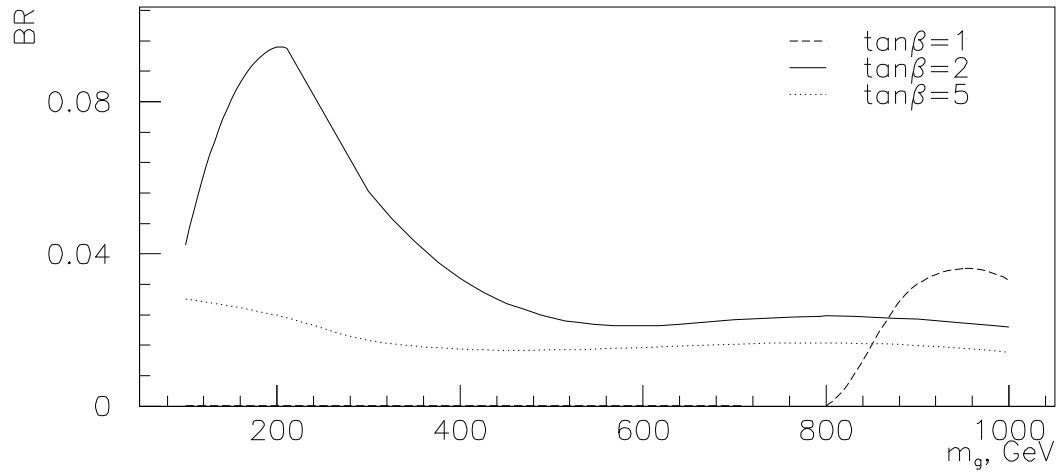


Fig. 14. $BR(\chi_2^0 \rightarrow \chi_1^0 \mu^+ \mu^-)$ vs m_g for $\mu = -200$ GeV.

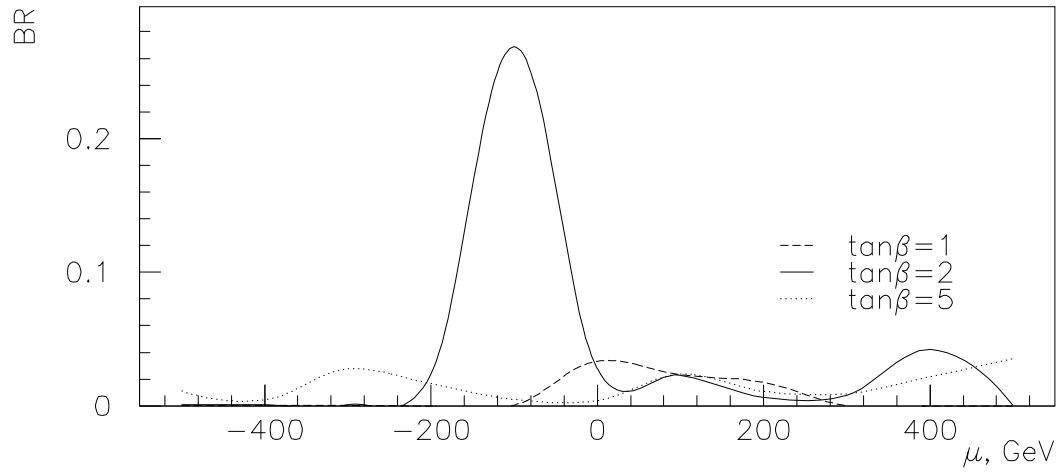


Fig. 15. $BR(\chi_2^0 \rightarrow \chi_1^0 \mu^+ \mu^-)$ vs μ for $m_g = 800$ GeV.

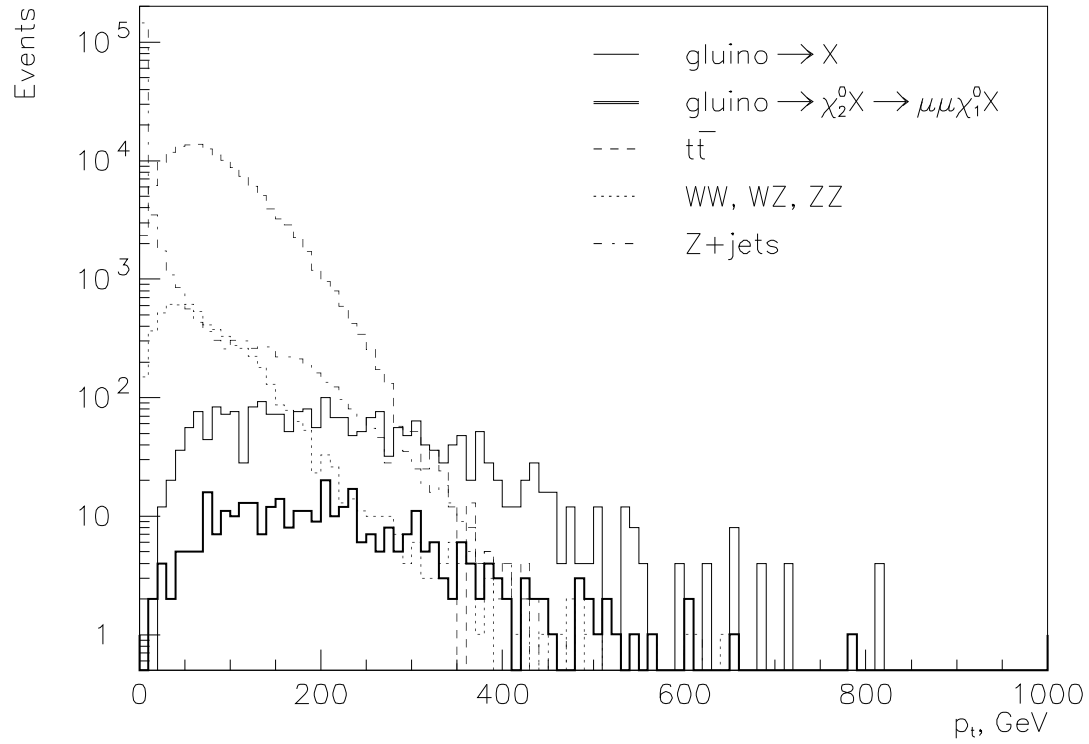


Fig. 16. Missing transverse momentum.

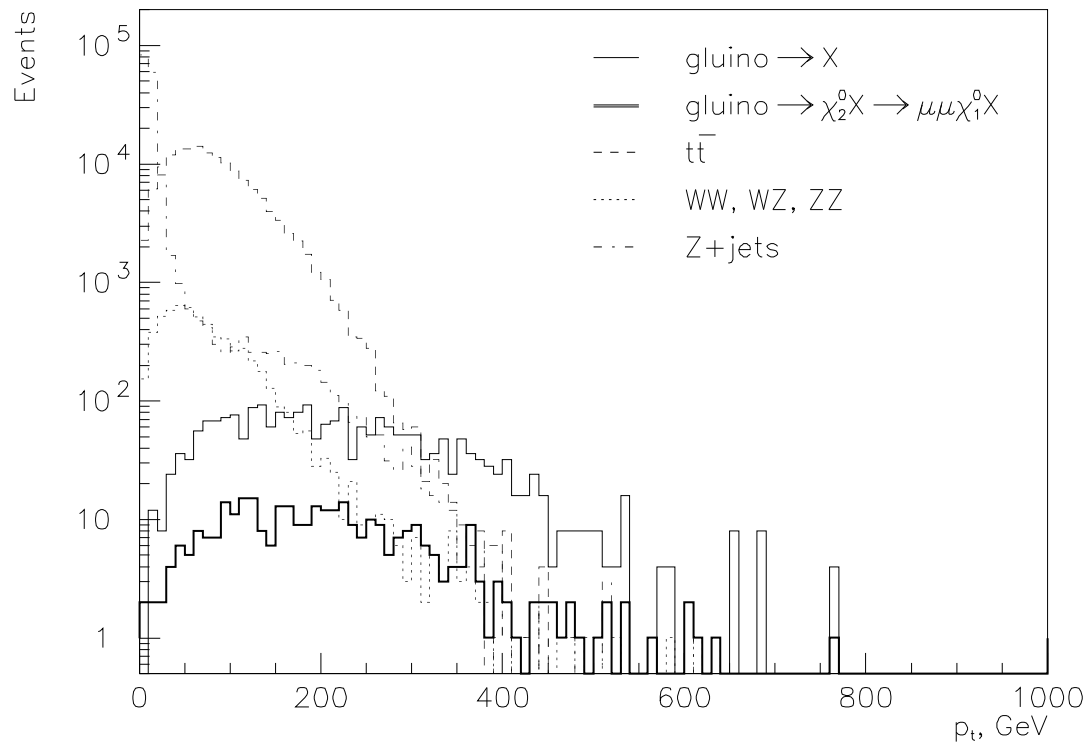


Fig. 17. Missing p_t over $-5 < \eta < 5$.

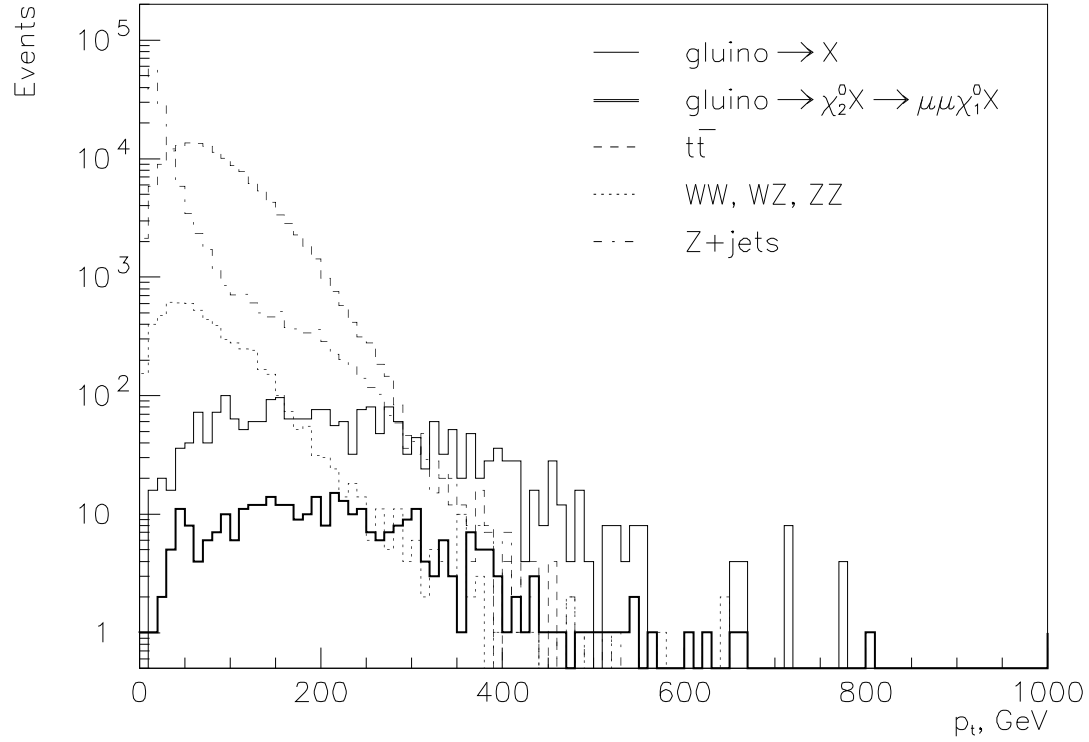


Fig. 18. Missing p_t from calorimeter over $-3 < \eta < 3$.

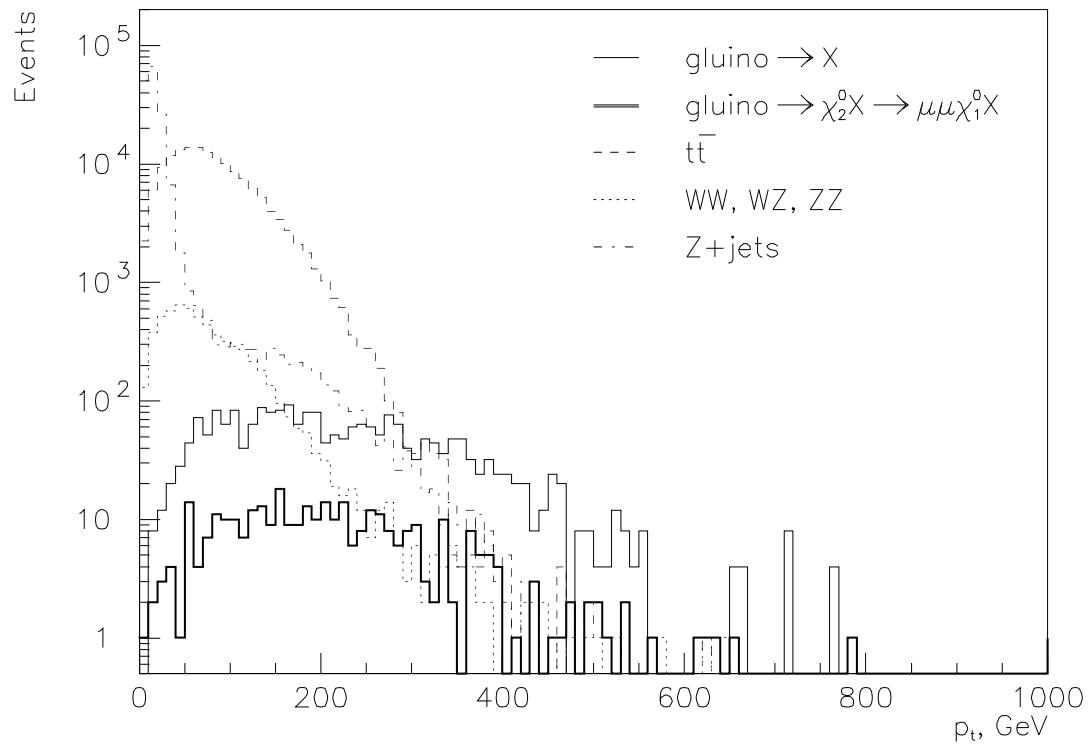


Fig. 19. Missing p_t from calorimeter over $-5 < \eta < 5$.

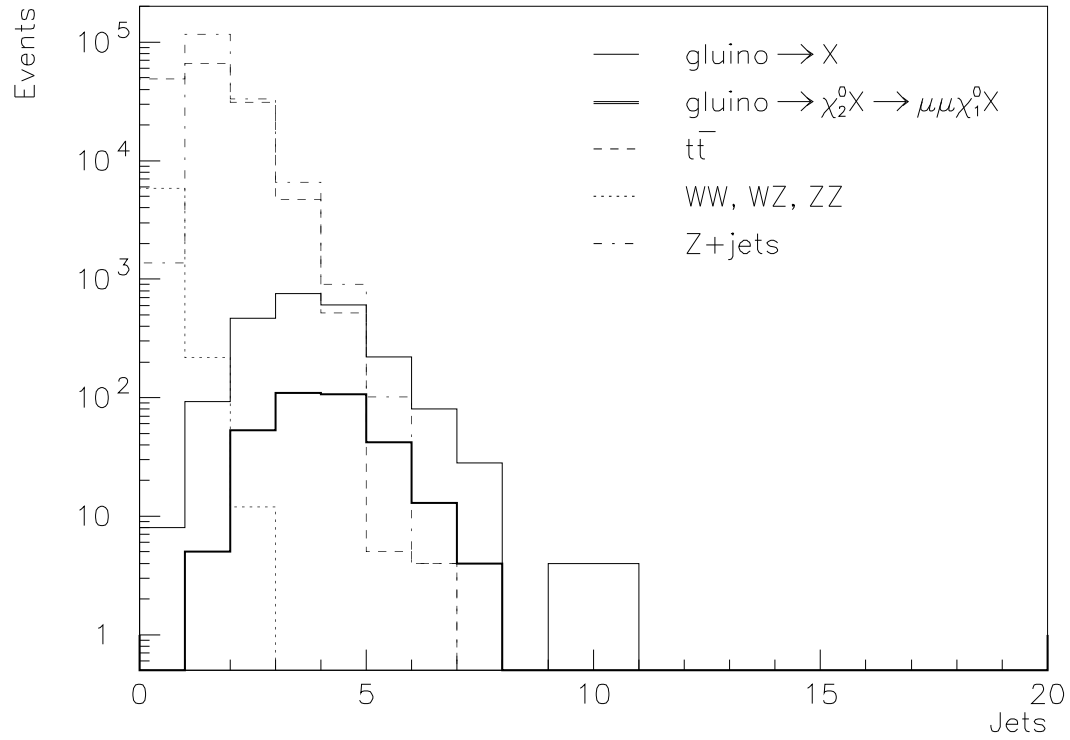


Fig. 20. Jet multiplicity for $E_t^j > 100$ GeV.

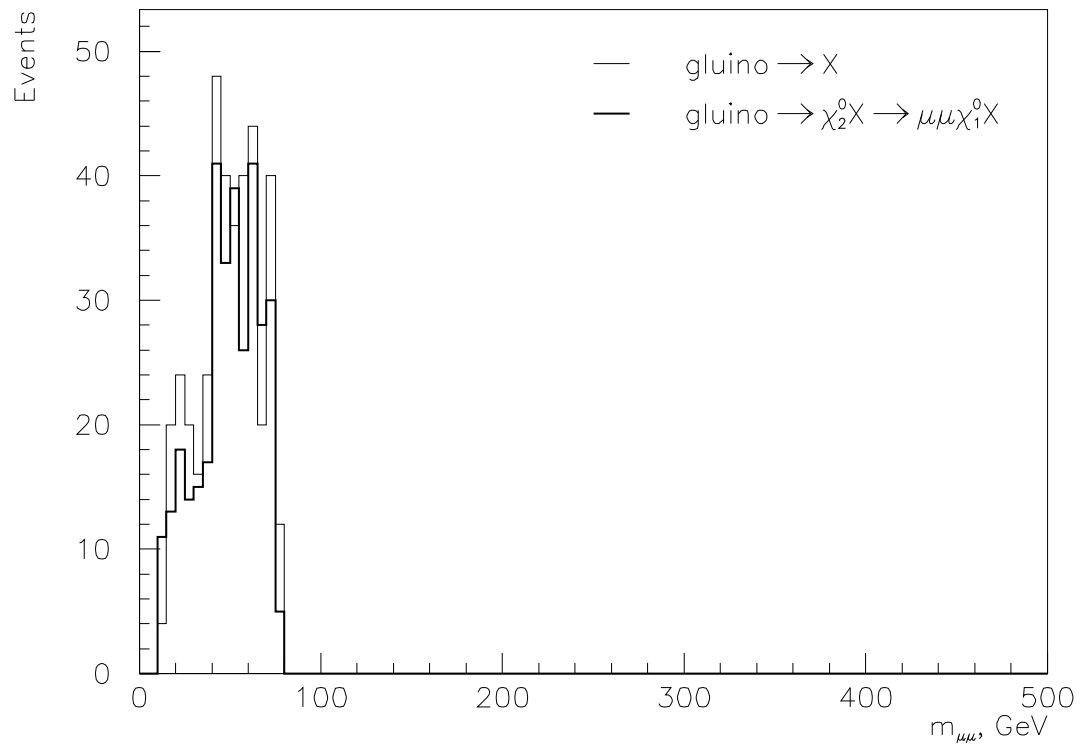


Fig. 21. χ_2^0 muon invariant mass.

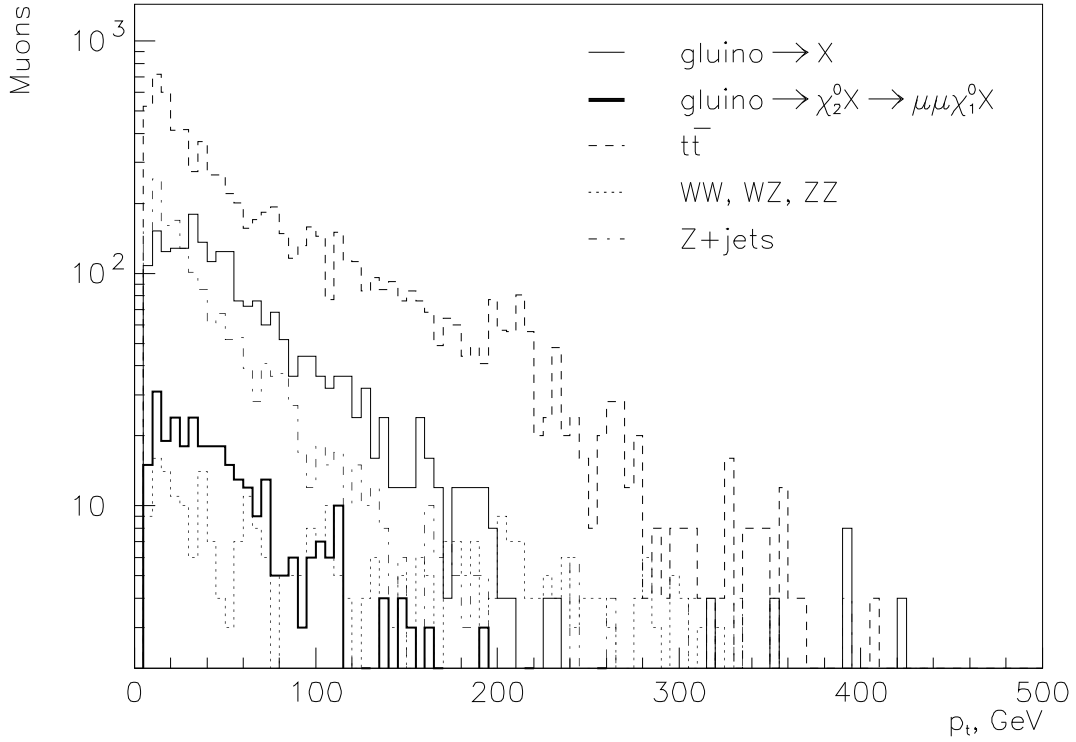


Fig. 22. Isolated muon p_t for $p_t^{\text{miss}} > 200$ GeV.

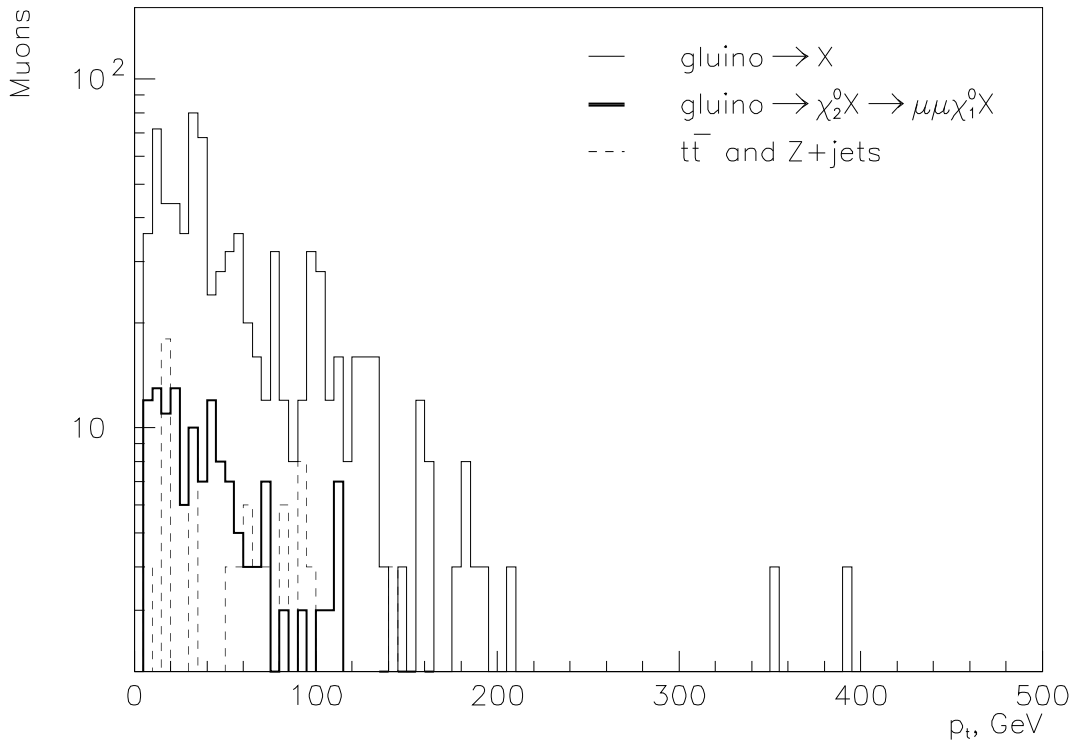


Fig. 23. Same as in Fig. 22, and for $n^j > 3$.

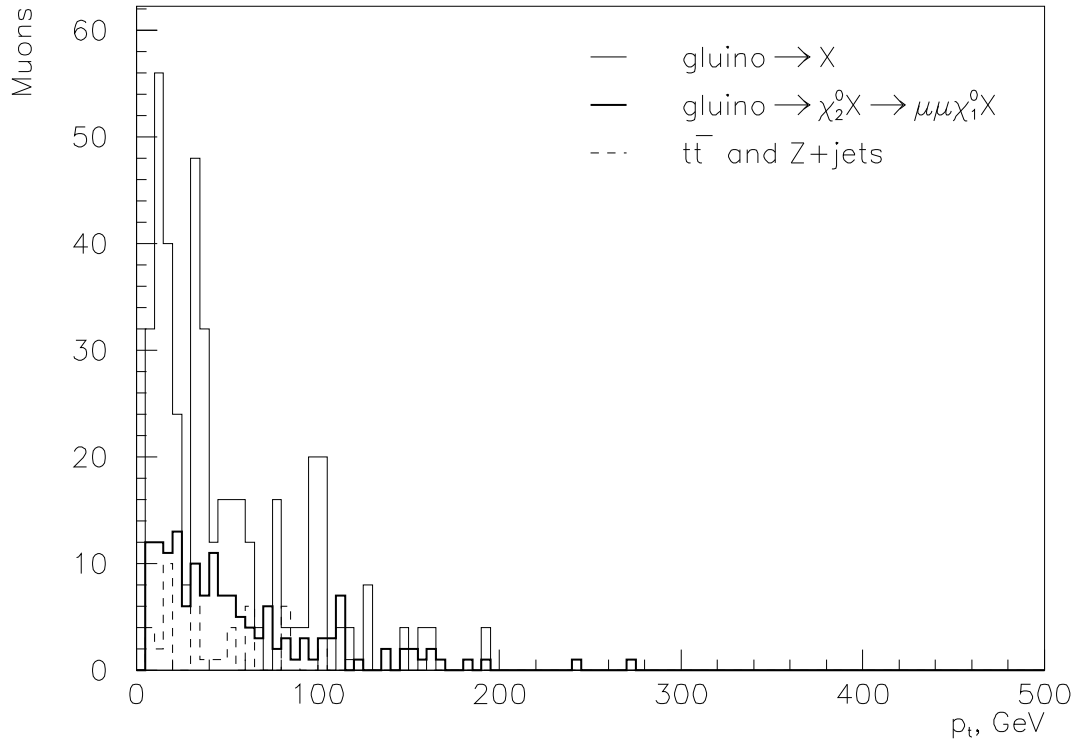
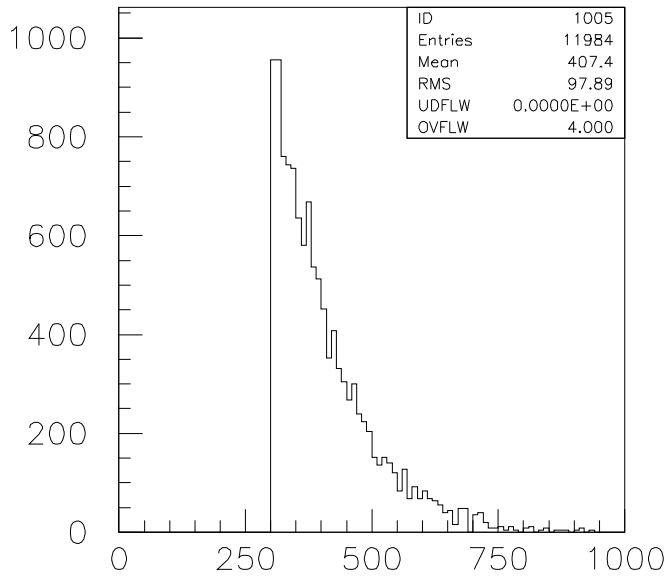
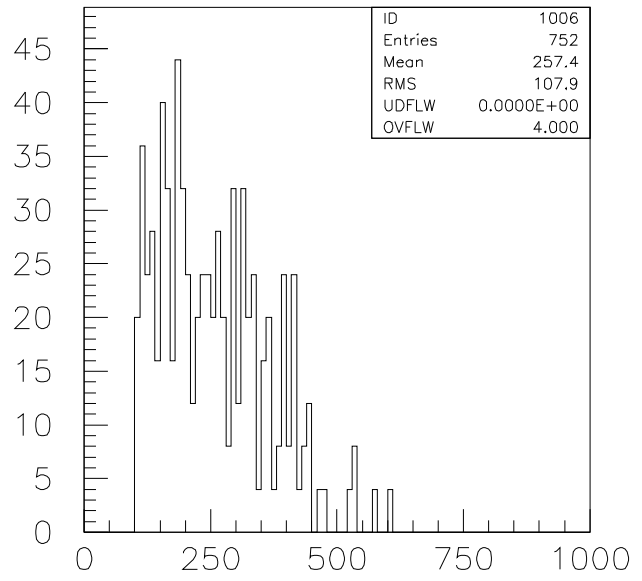


Fig. 24. Same as in Fig. 23, and for $m_{\mu\mu} < 80$ GeV.

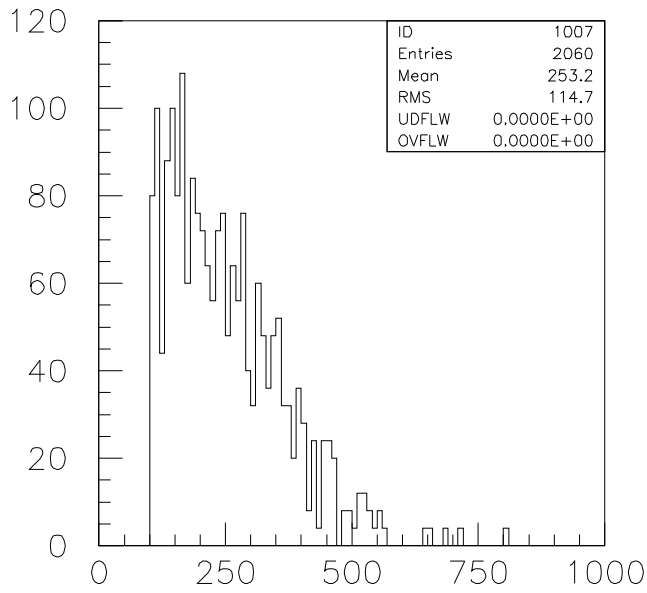
LHC \bar{g} 800 GeV \rightarrow X dec.



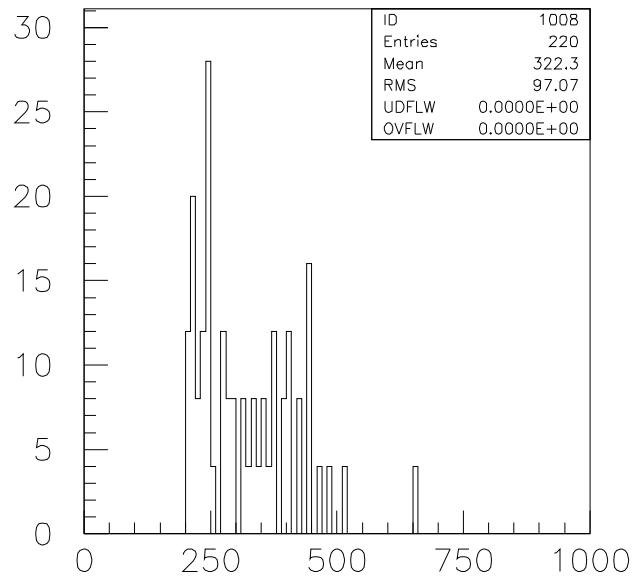
Missing E_t from calo (P-cuts)



Missing E_t from calo (KK-cuts, SS)



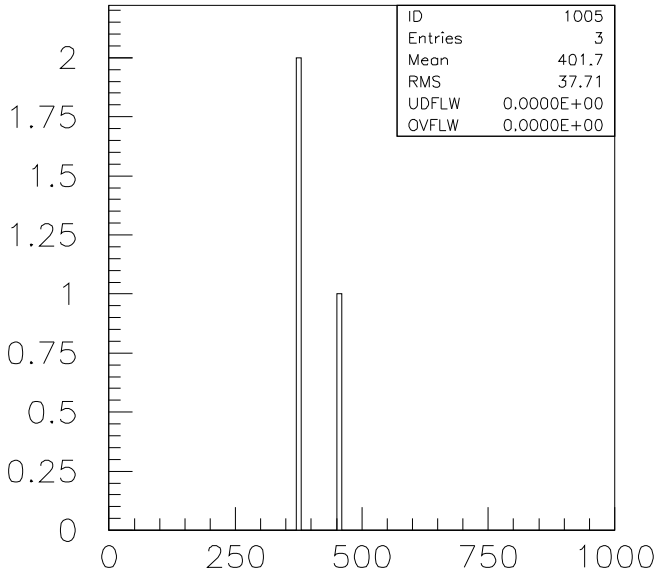
Missing E_t from calo (KK-cuts, OS)



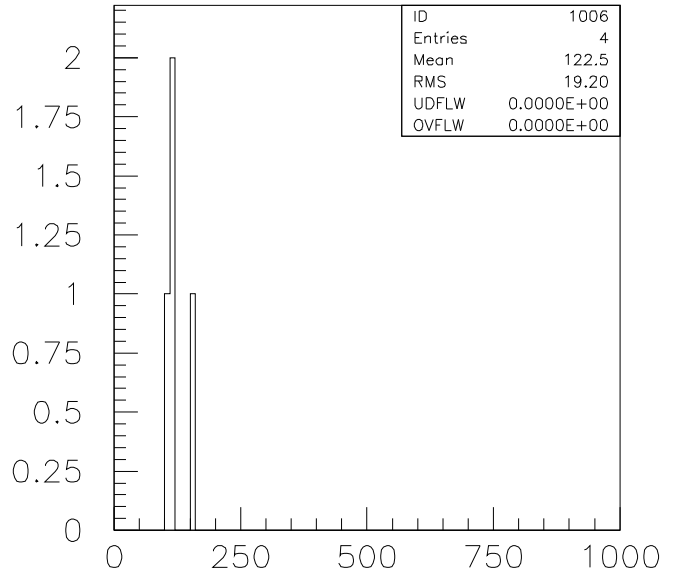
Missing E_t from calo (KNS-cuts, OS)

Fig. 25. Event missing transverse energy distribution for gluino signal for different sets of cuts.

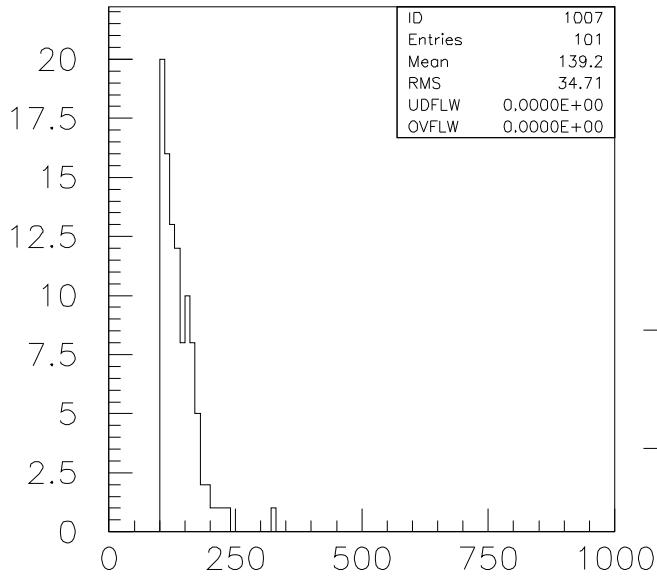
LHC $t\bar{t}$ 140 ($p_t=200$) GeV \rightarrow X bkg.



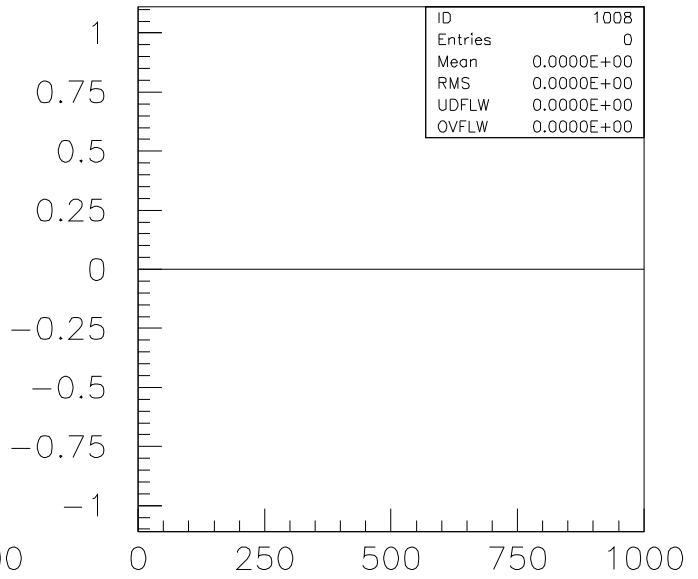
Missing E_t from calo (P-cuts)



Missing E_t from calo (KK-cuts, SS)



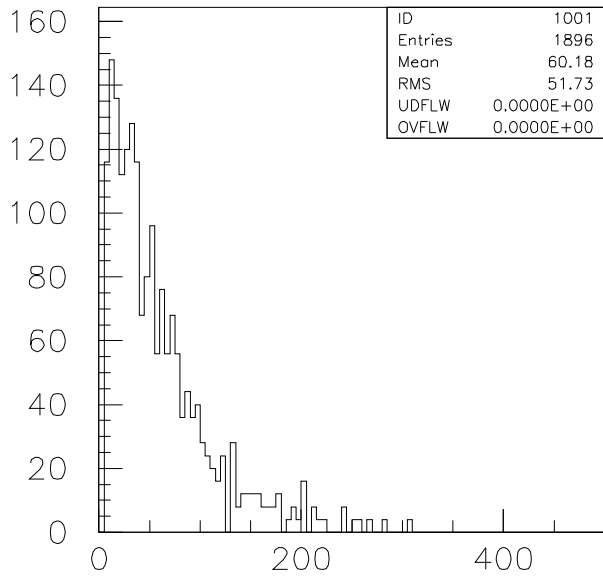
Missing E_t from calo (KK-cuts, OS)



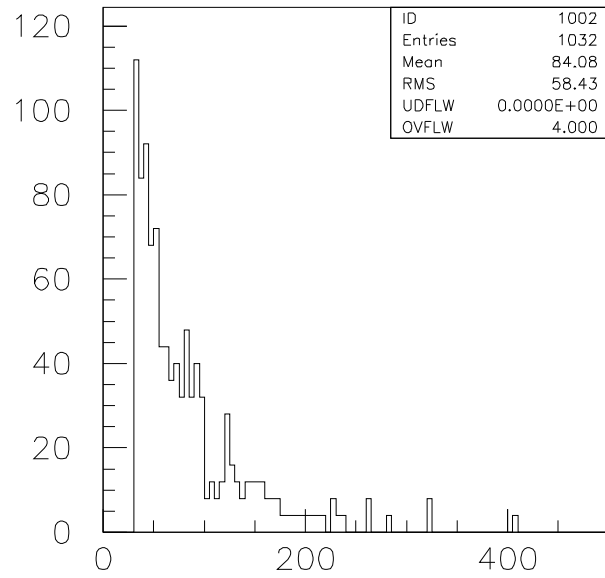
Missing E_t from calo (KNS-cuts, OS)

Fig. 26. Event missing transverse energy distribution for $t\bar{t}$ background for different sets of cuts.

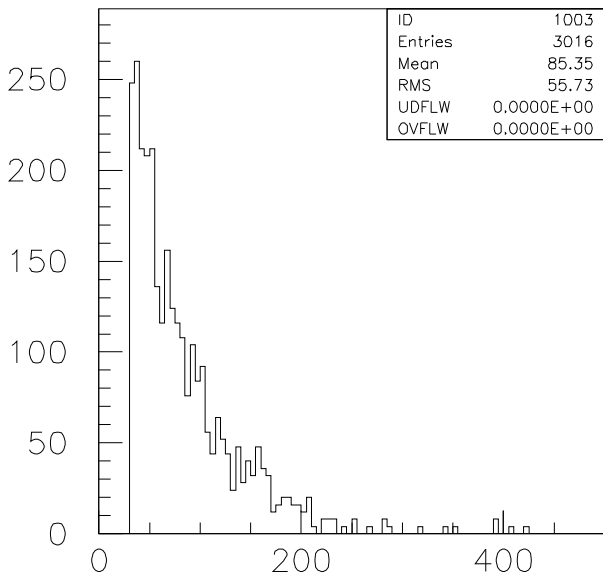
LHC \bar{g} 800 GeV \rightarrow X dec.



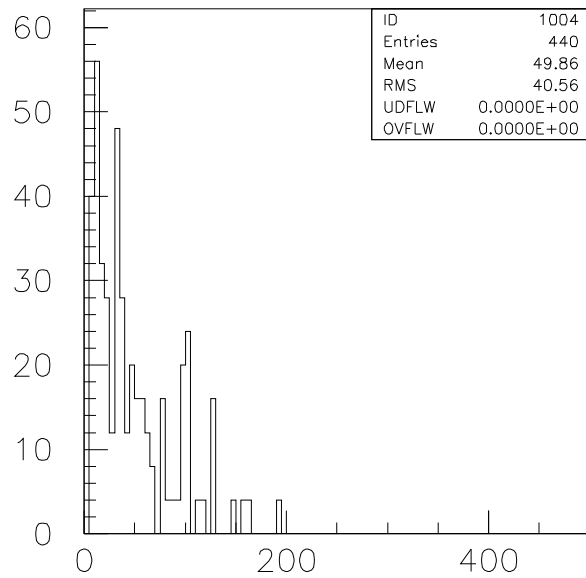
Isolated muon p_t (P-cuts, SS+OS)



Isolated muon p_t (KK-cuts, SS)



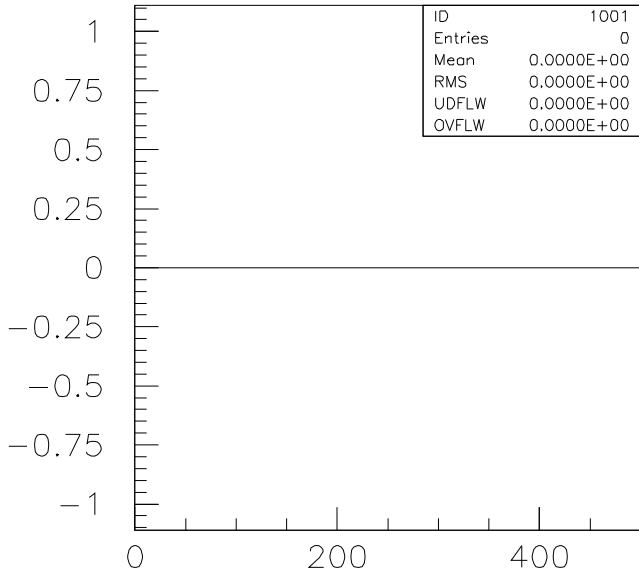
Isolated muon p_t (KK-cuts, OS)



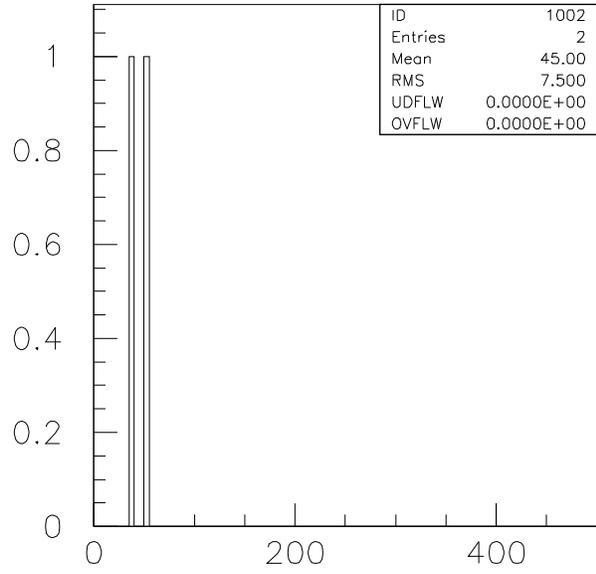
Isolated muon p_t (KNS-cuts, OS)

Fig. 27. Event missing transverse momentum distribution for gluino signal for different sets of cuts.

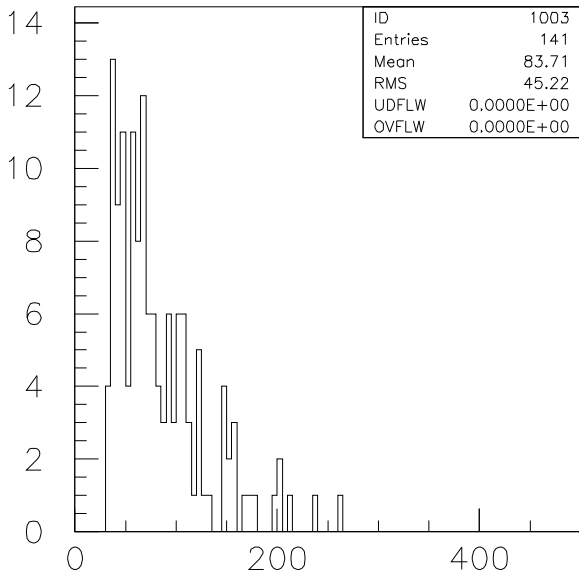
LHC $t\bar{t}$ 140 ($p_t=200$) GeV \rightarrow X bkg.



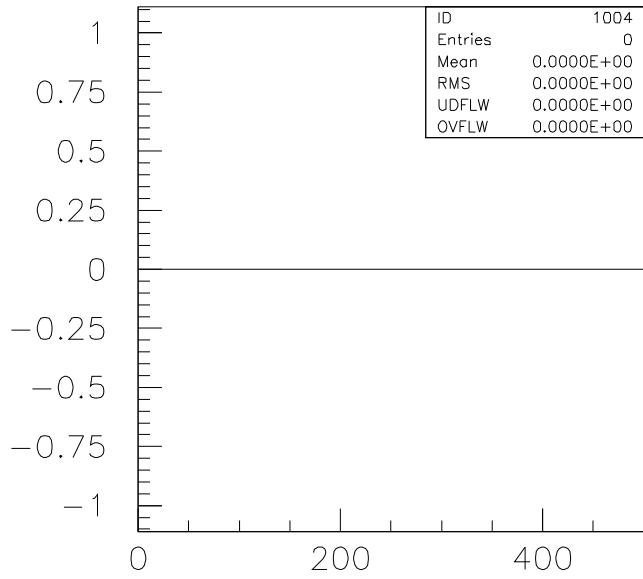
Isolated muon p_t (P-cuts, SS+OS)



Isolated muon p_t (KK-cuts, SS)



Isolated muon p_t (KK-cuts, OS)



Isolated muon p_t (KNS-cuts, OS)

Fig. 28. Event missing transverse momentum distribution for $t\bar{t}$ background for different sets of cuts.